Astron. Astrophys. 340, 527–542 (1998)

ASTRONOMY AND ASTROPHYSICS

Electron densities in planetary nebulae, and the unusual characteristics of the [S II] emission zone

J.P. Phillips

Instituto de Astronomia y Meteorologia, Avenida Vallarta 2602, Col. Arcos Vallarta, C.P. 44130 Guadalajara, Jalisco, Mexico
(e-mail: jpp@udgserv.cencar.udg.mx)

Received 19 June 1998 / Accepted 15 September 1998

Abstract. We investigate the radial variation of electron densities in planetary nebulae, using values of n_e deriving from the [S II] λ6717/λ6730 line ratio. As a result, we are able to show that there is a sharp discontinuity in densities of order 1.4 dex close to nebular radii $R = 0.1$ pc. It is proposed, as a consequence, that most nebulae contain two primary [S II] emission zones, with densities differing by a factor $\sim 10^2$. The intensity of emission from the denser component increases by an order of magnitude where nebulae pass from radiation to density-bound expansion regimes, resulting in a corresponding discontinuous jump in [S II]/Hβ line ratios.

The origins of these changes are not entirely clear, although one mechanism is investigated whereby the superwind outflows shock interact with exterior AGB envelopes.

Finally, the derived trends in $n_e(R)$ are used to determine distances for a further 262 nebulae. The resulting distance scale appears to be comparable to that of Daub (1982) and Cahn et al. (1992).

Key words: ISM: planetary nebulae: general – surveys

1. Introduction

The evolution of planetary nebular shells is thought to be divided into two primary phases. In the initial period of expansion, ionisation fronts propagate through the neutral "superwind" envelope, leading to a secularly increasing ionised mass M_i. Subsequently (for radii $R > 0.1$ pc) it is thought that the large majority of planetary nebulae are optically thin to ionising radiation, ionised shell masses are constant, and mean densities vary as R^{-3}.

Detailed investigations of shell evolution have been undertaken using a variety of codes and physical assumptions, and range from the early hydrodynamical modelling of Mathews (1966), and investigation of coupled dust-gas kinematics by Ferch & Salpeter (1975), to the two and three-wind models of Schmidt-Voigt & Köppen (1987a), Bedognil & D'Ercole (1986), Marten & Schönberner (1991) and Mellema (1994). It is apparent, from all of these analyses, that the radial density structures are expected to be a highly variable function of shell radius, depending as they do upon the shock interaction of superwind envelopes with interior stellar winds; of superwind envelopes with the exterior, relic AGB envelopes; and of course, upon the progress of ionisation fronts through the primary superwind outflow. In general however, it seems that both the peak and mean shell densities are expected to decline systematically as R increases.

Such a presumption appears to be confirmed through estimates of mean electron density by Schmidt-Voigt & Köppen (1987b); although evaluations of $n_e(R)$ are prone to a potentially broad range of uncertainties and errors. In particular, few PN distances (and therefore radii) are known to any degree of precision, whilst estimates of n_e based upon radio continuum/Hβ fluxes depend upon the nebular filling factor ε; a parameter which is open to many uncertainties, and may or may not vary with radius (see for instance the discussions of Mallik & Peimbert (1988); Kingsburgh & English (1992); and Kingsburgh & Barlow (1992)).

Values of n_e deriving from forbidden line ratios, by contrast, depend upon the roles of ionisation stratification and density gradients within the primary nebular envelopes, and the ranges of density over which the transition ratios may be used. Thus, it is possible that densities based upon [Cl III] λ5517/λ5537 and [Ar IV] λ4711/λ4740 line ratios are biased towards somewhat denser portions of the shells, including compact filaments and inclusions, whilst the [O II] λ3726/3729 and [S II] λ6717/6730 ratios yield densities typical of the nebular extremities, where both transitions are preferentially enhanced. As a consequence, the various transitions are likely to be biased towards differing sectors of the nebular shells, resulting in varying estimates of $\langle n_e \rangle$ (see Stanghellini & Kaler (1989) for a discussion of the transition dependency of n_e, and the more recent investigations of [O II]/[S II] density correlations by Kingsburgh & English (1992)).

In the following, we assess the relation between deduced and synthetic density functions $n_e(R)$ using [S II] λ6717/λ6730 line ratios alone. The subsequent close correlation between density and radius is then used to define a distance scale, and densities and distances are assessed for a further 262 sources. Finally, a comparison is made between the present distance scale, and

Send offprint requests to: J.P. Phillips

Table 1. Parameters for [S II] Calibration Nebulae

Source	Distance pc	Ref.	Radius arcsec	Radius pc	t	F(5 GHz) Jy	Log(n_e([S II])
NGC 246	450	1	112	0.24	1.58	0.248	2.30
NGC 1535	2700	2	9.2	0.12	1.17	0.166	3.72
NGC 2346	750	1	17	0.06	1.36	0.086	2.79
NGC 2392	2700	2	22.4	0.29	1.58	0.237	3.04
NGC 2440	885	3	9	0.04	1.40	0.411	2.79
NGC 2452	3230	3	9.4	0.15	1.17	0.055	3.40
NGC 2792	1930	3	6.5	0.06	1.48	0.116	3.52
NGC 2818	2300	5	20	0.22	1.52	0.033	2.84
NGC 3132	510	1	21	0.05	1.00	0.23	2.87
NGC 3211	1530	3	8	0.06	1.43	0.08	2.97
NGC 3242	420	1	18.6	0.04	1.13	0.835	3.50
NGC 3918	1790	3	9.4	0.08	1.25	0.8569	3.73
NGC 4361	1300	2	40.5	0.26	1.97	0.2303	2.48
NGC 5315	2820	3	3	0.04	0.92	0.415	4.29
NGC 6565	2640	3	4.5	0.06	1.04	0.042	3.27
NGC 6567	1530	3	4.4	0.03	1.10	0.161	4.25
NGC 6572	1700	6	2.7	0.02	1.03	1.4289	3.76
NGC 6578	2000	6	4.3	0.04	1.02	0.166	3.76
NGC 6629	2400	2	7.5	0.09	0.88	0.2658	3.14
NGC 6720	500	1	38	0.09	1.11	0.384	2.71
NGC 6741	1400	5	2.1	0.01	1.26	0.197	3.97
NGC 6803	3000	6	2.8	0.04	0.96	0.094	3.18
NGC 6853	360	1	165	0.29	1.10	1.3249	2.39
NGC 6884	1800	6	3.1	0.03	1.03	0.186	3.86
NGC 6886	1700	6	3	0.02	1.30	0.098	3.99
NGC 7009	2500	2	14.1	0.17	0.98	0.7355	3.78
NGC 7026	1450	5	7.5	0.05	0.91	0.277	3.52
NGC 7027	790	1	4.4	0.02	1.24	6.9211	4.13
NGC 7354	3430	5	10	0.17	1.22	0.5967	3.90
NGC 7662	790	1	7.6	0.03	1.28	0.634	3.50
He 2-138	5000	2	3.5	0.08	1.02	0.076	3.47
IC 418	2000	2	6.2	0.06	0.97	1.7332	4.02
IC 2448	4500	2	5	0.11	1.31	0.067	4.08
TC 1	3800	2	7.5	0.14	1.02	0.1472	3.24

Refs: 1. Pottasch (1996); 2. Mendez et al. (1989); 3. Cahn et al. (1992); 4. Pedreros (1989); 5. Kaler & Lutz (1985); 6. Gathier (1987)

those of Daub (1982), Cahn et al. (1992; hereafter CKS), Van de Steene & Zijlstra (1994; VdSZ), and Zhang (1995).

2. The distance and density calibration scale

For the purposes of this analysis, we have selected a total of 34 nebulae for which distances have been determined through model independent procedures; that is, through trigonometric and spectroscopic parallax, expansion distances, gravity distances, extinction distances and so forth. Details are provided in Table 1, where certain of the citations refer to prior compilations of model independent distances. Densities evaluated from the [S II] λ6717Å/λ6730Å ratio are taken from Barker (1978), Dufour (1984), Moran & Luise (1990), Barker (1984), Juguet et al. (1988), Khromov (1976), and particularly Stanghellini & Kaler (1989); where multiple measures are available, we have quoted a mean value $\langle \log n_e \rangle$.

Finally, we have estimated densities for five sources (NGC 6565; NGC 6578; NGC 7354; TC 1; and He 2-138) using [S II] ratios quoted by Kaler et al. (1997), the [S II] transition probabilities and collision strengths of Mendoza & Zeippen (1982) and Mendoza (1983), and electron temperatures from Cahn et al. (1992).

Although the density base is therefore somewhat heterogeneous, we believe that discrepancies arising from uncertain (and on occasion differing) estimates of electron temperature to be less than those arising from observational errors in the results; using the model results of Keenan et al. (1996), for instance, we determine $\Delta \log n_e \sim 0.02$ for $\Delta T_e/T_e \sim 0.1$. Much more serious *systematic* errors may arise due to uncertainties in ionic excitation rates and transition probabilities. Thus, following Keenan et al., an uncertainty in theoretical line ratios of $\Delta R_L/R_L \sim 0.2$ would translate into a typical error $\Delta \log n_e \sim 0.1$ in electron

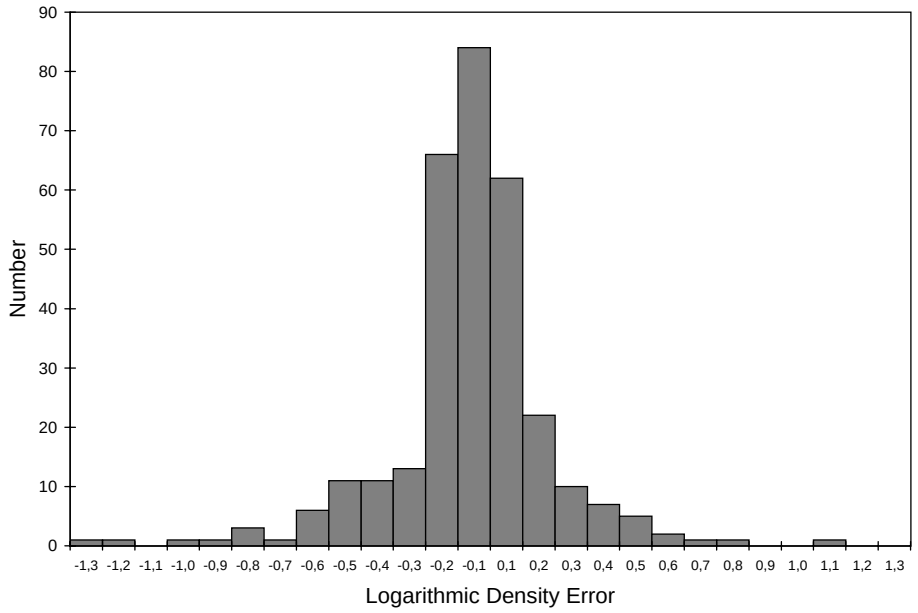

Fig. 1. Scatter of logarithmic densities about the mean as a result of errors in the evaluation of [S II] λ6717/λ6730, and density gradients in the nebular shells. The histogram is based upon 310 estimates of density in 128 nebulae

densities. The electron densities in Tables 1 and 3 may therefore be subject to systematic corrections of up to $\sim 25\%$. Note however that since similar ionic parameters are used for both the calibration nebulae and those listed in Table 3, such uncertainties have relatively little impact upon the trends noted in Fig. 2, or the distances listed in Table 3.

The accuracy of the [S II] line ratios is a strongly variable function of observational reference; although mean values deriving from multiple observations will, for the most part, be accurate to better than $\Delta \log n_e \cong 0.05$, values of n_e based on isolated measurements can be trusted to no better than $\Delta \log n_e \cong 0.1$. These errors alone are probably insufficient to bias trends in $n_e(R)$ to any appreciable degree (see Sect. 3).

A potentially more serious problem arises from the fact that differing density estimates may correspond to differing parts of the nebular shell; none of the [S II] ratios are based on integrated fluxes for the entire nebula. Since electron density is often a function of projected shell location (e.g. Phillips & Cuesta 1996), it follows that the quoted values of log n_e may be unrepresentative of the shell as a whole.

The extent of this uncertainty may, fortunately, be assessed by comparing densities in nebulae for which multiple observations are available. For this purpose, we have used a total of 310 observations of the [S II] line ratio summarised Kaler et al. (1997), corresponding to 128 individual sources. A mean logarithmic density is defined through $\langle \log n_e \rangle_i = n^{-1} \sum_j [\log n_e]_{ij}$, where the summation corresponds to the j individual estimates of $\log n_e$ in source i. Finally we evaluate for each source i, and each density estimate j a function $\Delta n = (\log n_e)_{ij} - \langle \log n_e \rangle_i$, representing the difference from the mean of any individual density $(\log n_e)_{ij}$. A summed histogram of Δn for all $i = 128$ sources is illustrated in Fig. 1.

It is apparent, from this, that there is indeed a scatter in the estimates of $\log n_e$, arising from both changes in electron density through the shells, and variations in the accuracies of the observations. In the mean, however, the range of uncertainty appears to be of order $\Delta \log n_e = 0.15$. That is, the variation in n_e over the nebular shells is typically less than 40% for the sizes of aperture used in these observations. Note, however, that there is evidence to favour significantly larger variations in n_e where spatial resolutions are higher (e.g. Juguet et al. 1988; Moran & Luise 1990; Phillips & Cuesta 1996; Phillips & Cuesta 1998).

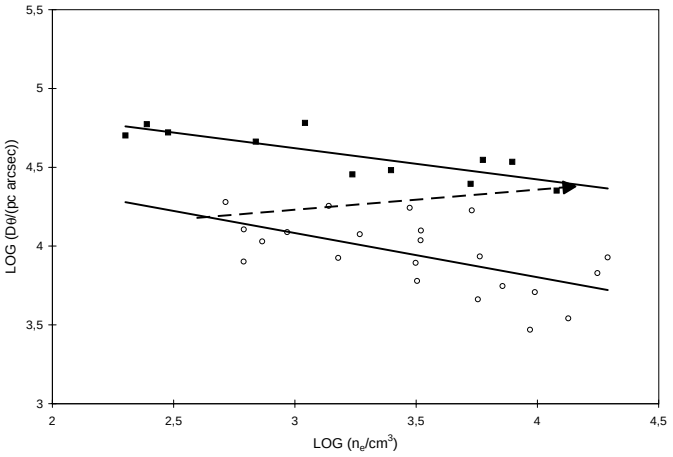

Fig. 2. Variation of $D\theta$ with density n_e in 32 nebulae having reasonably well established distances, and measured line ratios [S II] λ6717/λ6730. The two diagonal lines represent least-squares fits to nebulae having $R \leq 0.1$ pc (○) and $R > 0.1$ pc (■). Note that the two sequences are distinct, and separated by a density discontinuity of size ~ 1.4 dex

In comparing densities with radial sizes (see Sect. 3) we should also note two further important sources of error. The first of these, the error in distance, is very difficult to assess with any confidence, although it is unlikely (in the mean) to exceed $\Delta \log(d) \sim 0.1$. A potentially more serious problem

may however arise from uncertainties in angular diameter Θ. In particular, nebulae are often characterised by a hierarchy of structures, and it may be difficult to establish which outflow shell yields the most appropriate angular radius. In addition, a large fraction of sources appear to be appreciably non-spherical, whilst very small nebulae (those having <2.5 arcsec) are prone to proportionately greater errors $\Delta\theta/\theta$.

We shall see, later, that there is indeed evidence for random variations in θ consistent with errors $\langle\Delta\theta/\theta\rangle \sim 0.35$. For present purposes, we have attempted to alleviate this problem by including only those sources having $\theta > 2.5$ arcsec.

Even allowing for this, however, care must be taken in interpreting gradients between $\log D\theta$ and $\log n_e$ (Sect. 3), since they may be appreciably modified through such uncertainties (see, for instance, the related discussion of filling factors ε by Kingsburgh & English (1992)).

Finally, and as is well known, the range in [S II] ratios over which densities may be reliably evaluated is restricted. Three of the sources (NGC 6567, NGC 5315, and NGC 7027) have [S II] ratios falling somewhat outside these limits, and errors in deduced densities are likely to be correspondingly greater. Elimination of these sources, however, would affect neither the mean trends in density, nor the analyses in Sects. 3 and 4.

3. The radial variation in nebular densities

The relation between the parameter log $D\theta$ and $\log n_e$ is illustrated in Fig. 2 (where it may be noted that $(R/\mathrm{pc}) = 4.85\ 10^{-6}(D/\mathrm{pc})(\theta/\mathrm{arcsec})$). It may be seen, from this, that whatever might have been supposed from theoretical analyses, there is in fact no simple relation between $\log n_e$ and log R. Specifically, we find that

– sources optically thick to Lyman continuum ionising radiation (i.e. those having $R \leq 0.1$ pc; see for instance Daub (1982) and Cahn et al. (1992)) follow a least squares relation

$$\log\left[\frac{D\theta}{\mathrm{pc\ arcsec}}\right] = -0.281 \log\left[\frac{n_e}{\mathrm{cm}^{-3}}\right] + 4.925\ldots \quad (1)$$

The scatter about this trend is relatively large, resulting in a correlation coefficient $r = 0.60$.

– sources having $R > 0.1$ pc follow the differing relation

$$\log\left[\frac{D\theta}{\mathrm{pc\ arcsec}}\right] = -0.198 \log\left[\frac{n_e}{\mathrm{cm}^{-3}}\right] + 5.216\ldots \quad (2)$$

Although the number of (optically thin) sources is restricted, it appears that there is significantly less scatter about the least-squares trend than for $R \leq 0.1$ pc, and the correlation coefficient is correspondingly larger ($r = 0.82$).

– There is a discontinuity in densities close to $R = 0.1$ pc ($\log D\theta = 4.31$), such that densities for larger nebulae are 1.4 dex greater than those for smaller sources.

Within errors, therefore, radial density gradients dn_e/dR for optically thick and thin sources are comparable – and very much greater than might have been anticipated from the nebular models described in Sect. 1.

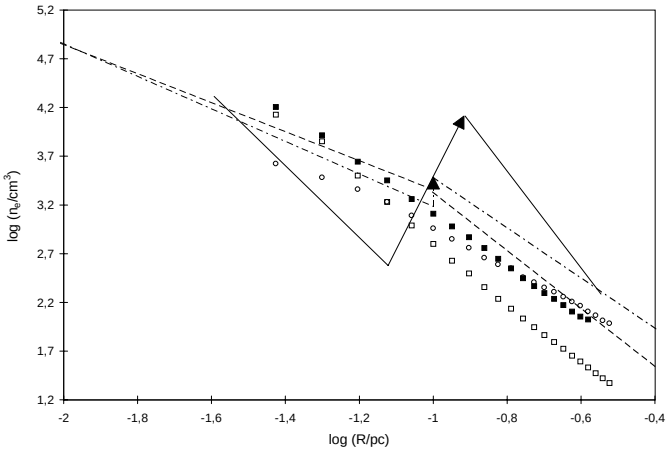

Fig. 3. Comparison of the mean [S II] (_____) and radio continuum (– . – . – .) density variations with the accreting three wind (■), non-accreting three wind (□), and two wind (○) models of Schmidt-Voigt & Köppen (1987a). Also shown is the variation expected for a simple homogeneous model, in which the central star ionising flux is constant (- - - - - -).

In addition, a direct comparison between present trends and those deriving from the two and three-wind models of Schmidt-Voigt & Köppen (1987a) (Fig. 3) suggests that there is no synthetic counterpart of the discontinuities described above; all of the model densities fall systematically and regularly with radius. Similarly, perusal of the model structures of Schmidt-Voigt & Köppen (1987a) and Marten & Schonberner (1991) implies that peak shell densities n_e (peak) vary in a similar manner; although n_e (peak) may at various times refer to the principal ionisation front, and interior shocked stellar wind.

Some caution is of course required in interpreting such trends, as was noted in Sect. 2. There is however no easy way of reconciling theoretical expectations with the apparent jump in densities close to $R \cong 0.1$ pc. We can only suppose that, for whatever reason, there is a species of phase change close to the boundary between optically thick and thin sources (i.e. radiation and density-bound nebulae). So extreme is this effect, indeed, that it is pertinent to ask whether other, related discontinuities might be associated with this transition.

To investigate this, we have de-reddened 587 line ratios [S II]/Hβ from the compilation of Kaler et al. (1997), using the extinction coefficients of Tylenda et al. (1992). The variation of these ratios with nebular radius is then assessed through comparison with the radius estimates of CSK, and radii to be evaluated in Sect. 5 (see Table 3).

As may be seen from Fig. 4, the data sets differ in certain crucial respects. Thus, for instance, the trend based upon current radius estimates appears to be characterised by an absence of sources close to the $R = 0.1$ pc; a distribution which reflects the difficulty in acquiring reliable [S II] densities close to the optically thick/thin transition (see Fig. 2, where it will be noted that $\log n_e$ may take values > 4 or < 2.5 depending upon the optical thickness of the source).

Table 2. Parameters for 5 GHz Calibration Nebulae

Source	Distance pc	Ref.	Radius arcsec	Radius pc	t	F(5 GHz) Jy	He+/H	He++/H	LOG($n_e\varepsilon^{0.5}$) cm^{-3}
NGC 246	450	1	112	0.24	1.58	0.248	0.059	0.056	1.97
NGC 650	720	1	69.2	0.24	1.07	0.11	0.076	0.032	1.99
NGC 1360	420	1	192	0.39	1.65	0.222	0.061	0.049	1.62
NGC 1514	550	1	50.2	0.13	1.08	0.262	0.096	0.014	2.46
NGC 1535	2700	2	9.2	0.12	1.17	0.166	0.085	0.011	3.13
NGC 2346	750	1	17	0.06	1.36	0.086	0.119	0.017	2.87
NGC 2392	2700	2	22.4	0.29	1.58	0.237	0.064	0.028	2.64
NGC 2440	885	3	9	0.04	1.40	0.411	0.106	0.042	3.57
NGC 2452	3230	3	9.4	0.15	1.17	0.055	0.074	0.040	2.82
NGC 2792	1930	3	6.5	0.06	1.48	0.116	0.068	0.048	3.35
NGC 2818	2300	5	20	0.22	1.52	0.033	0.072	0.038	2.31
NGC 3132	510	1	21	0.05	1.00	0.23	0.114	0.012	3.01
NGC 3211	1530	3	8	0.06	1.43	0.08	0.104	0.048	3.17
NGC 3242	420	1	18.6	0.04	1.13	0.835	0.081	0.019	3.42
NGC 3587	500	1	100	0.24	1.09	0.091	0.073	0.008	1.81
NGC 3918	1790	3	9.4	0.08	1.25	0.8569	0.083	0.025	3.56
NGC 4361	1300	2	40.5	0.26	1.97	0.2303	0.072	0.059	2.40
NGC 5189	1730	6	16	0.13	1.27	0.356	0.078	0.032	3.02
NGC 5315	2820	3	3	0.04	0.92	0.415	0.121	0.006	4.03
NGC 6369	2000	6	19	0.18	1.25	1.907	0.105	0.005	3.26
NGC 6537	2400	6	2.4	0.03	1.57	0.61	0.213	0.057	4.28
NGC 6565	2640	3	4.5	0.06	1.04	0.042	0.130	0.010	3.28
NGC 6567	1530	3	4.4	0.03	1.10	0.161	0.120	0.002	3.72
NGC 6572	1700	6	2.7	0.02	1.03	1.4289	0.109	0.000	4.49
NGC 6578	2000	6	4.3	0.04	1.02	0.166	0.108	0.002	3.68
NGC 6629	2400	2	7.5	0.09	0.88	0.2658	0.130	0.000	3.37
NGC 6720	500	1	38	0.09	1.11	0.384	0.087	0.026	2.74
NGC 6741	1400	5	2.1	0.01	1.26	0.197	0.103	0.033	4.26
NGC 6803	3000	6	2.8	0.04	0.96	0.094	0.123	0.003	3.74
NGC 6853	360	1	165	0.29	1.10	1.3249	0.087	0.023	2.12
NGC 6884	1800	6	3.1	0.03	1.03	0.186	0.106	0.008	3.94
NGC 6886	1700	6	3	0.02	1.30	0.098	0.084	0.028	3.84
NGC 6891	3800	2	10.2	0.19	1.02	0.103	0.112	0.000	2.88
NGC 6894	1040	5	27.5	0.14	1.02	0.061	0.103	0.007	2.39
NGC 7009	2500	2	14.1	0.17	0.98	0.7355	0.099	0.013	3.17
NGC 7026	1450	5	7.5	0.05	0.91	0.277	0.094	0.008	3.49
NGC 7027	790	1	4.4	0.02	1.24	6.9211	0.082	0.029	4.68
NGC 7293	280	1	402	0.55	1.10	1.292	0.182	0.008	1.59
NGC 7354	3430	5	10	0.17	1.22	0.5967	0.089	0.028	3.29
NGC 7662	790	1	7.6	0.03	1.28	0.634	0.076	0.031	3.81
IC 418	2000	2	6.2	0.06	0.97	1.7332	0.076	0.000	3.96
IC 289	1870	5	6.2	0.06	1.55	0.212	0.061	0.049	3.52
IC 1747	2200	5	6.5	0.07	1.01	0.128	0.094	0.013	3.33
IC 2448	4500	2	5	0.11	1.31	0.067	0.074	0.021	3.22
IC 4637	1600	2	9.3	0.07	1.02	0.013	0.109	0.000	2.67
A 7	550	1	382	1.02	1.02	0.305	0.092	0.018	1.16
A 24	600	1	177.4	0.52	1.02	0.036	0.092	0.018	1.18
A 31	400	1	486	0.94	1.16	0.102	0.088	0.022	0.84
A 33	1260	1	134	0.82	1.16	0.014	0.075	0.035	1.00
A 35	200	1	386	0.37	1.02	0.255	0.092	0.018	1.34
A 36	500	1	183.5	0.44	1.70	0.174	0.059	0.055	1.56
A 39	1580	1	87	0.67	1.37	0.0057	0.071	0.039	1.04
Ha 2-1	4600	2	1.1	0.02	1.02	0.065	0.108	0.002	4.19
He 2-36	780	1	11	0.04	1.65	0.0751	0.056	0.054	3.11
He 2-108	8300	2	5.5	0.22	0.97	0.033	0.101	0.000	2.86

Table 2. (continued)

Source	Distance pc	Ref.	Radius arcsec	Radius pc	t	F(5 GHz) Jy	He+/H	He++/H	LOG($n_e\varepsilon^{0.5}$) cm^{-3}
He 2-131	610	3	3	0.00	1.02	0.335	0.035	0.000	4.34
He 2-138	5000	2	3.5	0.08	1.02	0.076	0.011	0.000	3.47
Jn 1	800	1	166	0.64	1.25	0.0098	0.078	0.032	0.89
K 1-16	1700	1	47	0.39	1.81	0.0759	0.054	0.056	2.01
M 1-26	1900	2	1.5	0.01	1.02	0.451	0.109	0.000	4.60
PHL 932	520	1	135	0.34	2.02	0.0088	0.092	0.018	1.13
PW 1	300	1	1200	1.75	1.19	0.0847	0.092	0.018	0.28
TC 1	3800	2	7.5	0.14	1.02	0.1472	0.110	0.000	3.15
VV 47	900	1	190	0.83	1.13	0.019	0.094	0.020	0.91

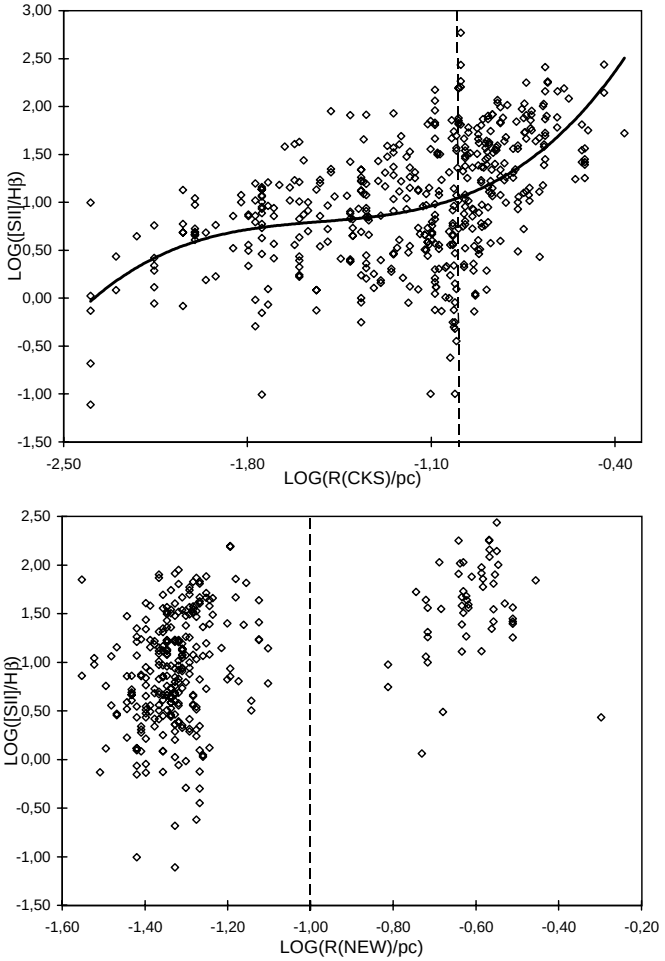

Fig. 4. Variation of the ratio [S II]/Hβ with nebular radius (where in this figure alone, I(Hβ) has been normalised to a value of 10^2). Two correlations are shown, corresponding to the radii of CKS, and those derived in the present paper (R(NEW)), whilst the curve in the former diagram corresponds to a third order polynomial least squares fit. Note that both figures indicate a more-or-less discontinuous variation of I([S II])/Hβ close to $R = 0.1$ pc

Both sets of data, however, show an appreciable change in I([S II])/I(Hβ) close to $R = 0.1$ pc. The nature of this variation is not clearly defined; the 3$^{\rm rd}$ order regression function illustrated in Fig. 4, for instance, might suggest a steepening in gradients $d(\log \mathrm{I([S\,II])})/d(\log R)$ for larger nebulae. More simply and plausibly, however, we believe that the trends in Fig. 4 are also consistent with a discontinuous change in I([S II])/I(Hβ). The size of this change may be assessed by evaluating a ratio u, where $\log u = \langle \log(\mathrm{I([S\,II])/I(H}\beta))\rangle_{R>0.1\,\mathrm{pc}} - \langle \log(\mathrm{I([S\,II])/I(H}\beta))\rangle_{R<0.1\,\mathrm{pc}}$ – that is, u represents the ratio between the (logarithmic mean) fluxes for larger nebulae, and those for smaller nebulae. Depending upon the distance scale employed, we then find $u = 4.90\pm^{0.95}_{0.80}$ (Daub); $3.86\pm^{0.57}_{0.50}$ (CKS); and $4.85\pm^{0.88}_{0.75}$ (present values of radius, Table 2). It appears, in brief, that whichever distance scale one chooses to select, the jump in line intensity (relative to Hβ) is generally the same, and of order $\sim$5.

From the foregoing, therefore, it is clear that the [S II] emission lines are associated with two principal discontinuities at $R = 0.1$ pc, relating to line intensity and density.

Finally, it is interesting to compare the density values in Fig. 2 with mean shell densities derived from 5 GHz fluxes. We shall assume for this purpose that nebulae are spherically symmetric, and characterised by a volume filling factor ε. Under these circumstances, it is readily shown that the radio continuum flux at frequency ν GHz would be given by

$$F(\nu) = 1.2110^{-12} T_e^{-0.35} \nu^{-0.1} n_e n(H)\, \varepsilon Y \left[\frac{D}{\mathrm{pc}}\right] \times \left[\frac{\theta}{\mathrm{arcsec}}\right]^3 \mathrm{Jy}$$

where

$$Y = \left[1 + \frac{n(He^+)}{n(H^+)} + \frac{4n(He^{++})}{n(H^+)} \frac{\ln\left(4.9510^{-2} T_e^{1.5} \nu^{-1}\right)}{\ln\left(9.910^{-2} T_e^{1.5} \nu^{-1}\right)}\right]$$

To a very good approximation we may therefore write

$$n_e\,(\mathrm{rms}) = 4.9510^6 \left[\frac{F\,(5\,\mathrm{GHz})}{\mathrm{Jy}}\right]^{0.5} t^{0.175} Y^{-0.5} \left[\frac{D}{\mathrm{pc}}\right]^{-0.5} \times \left[\frac{\theta}{\mathrm{arcsec}}\right]^{-1.5} \varepsilon^{-0.5}\,\mathrm{cm}^{-3}$$

It follows, from this, that n_e (rms) represents a (root mean square) value for the radio continuum emission regime; that is,

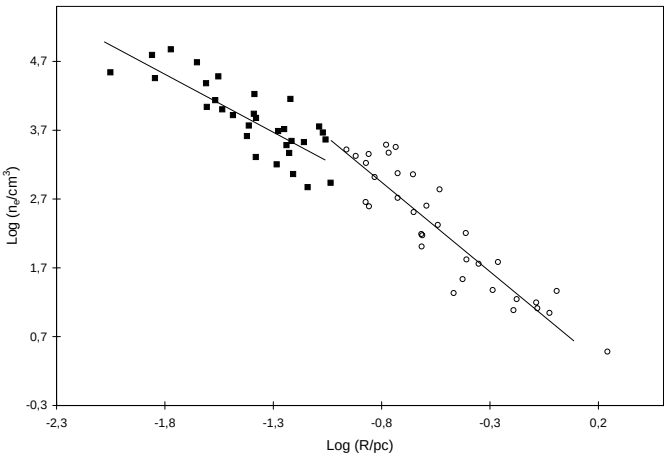

Fig. 5. The variation of the root mean square density as a function of ionised nebular radius R (see text for details). The two diagonal lines correspond to least-squares fits for nebulae having $R \leq 0.1$ pc (■) and $R > 0.1$ pc (○)

the primary nebular ionised mass. [S II] densities by contrast appear to be representative of the peripheries of the sources, where both [O II] and [S II] transitions are preferentially enhanced.

The variation of n_e (rms) is illustrated in Fig. 5 for a total of 64 nebulae having reasonably well established distances (see Table 2; where numbers in column 3 correspond to the references cited in Table 1). We have employed values of $n(\mathrm{He}^+)/n(\mathrm{H}^+)$, $n(\mathrm{He}^{++})/n(\mathrm{H}^+)$, and $t = T_e/10^4$ K from Cahn et al. (1992), of F(5 GHz) from Milne & Aller (1975) and other sources (see references cited in Sect. 5), and assumed a mean value $\varepsilon = 0.4$ based on the analyses of Kingsburgh & English (1992) and Boffi & Stanghellini (1994). We have also separately indicated linear least-squares solutions for small and large nebulae.

It is immediately apparent from this that, unlike the case of [S II], there is no appreciable change in density close to $R = 0.1$ pc. At the most, it is possible to claim a variation of ~ 0.3 dex in n_e.

Such a result is broadly consistent with the theoretical models of Schmidt-Voigt & Köppen (1987a) and Marten & Schonberner (1991), whence it is apparent that there is little change in gradient dn_e/dR close to $R = 0.1$ pc. It may also be noted that whilst there is little to support a discontinuity in densities, there is clear evidence for a change in gradient dn_e/dR between smaller ($R \leq 0.1$ pc) and larger nebulae. Such gradients are also reasonably well replicated by the two winds model of Schmidt-Voigt & Köppen (1987a) and (for the smaller nebulae at least) by a simple homogeneous expanding model, in which the ionising flux is assumed invariant, and ionised mass M_i varies as $n_e\ R^3$ for $R \leq 0.1$ pc. The displacement between certain of the synthetic models and the 5 GHz results should not be regarded as unduly significant.

Stasinska (1989) has also modelled trends in $n_e(R)$ for planetary nebulae, as a result of which mean densities are found to decrease more-or-less discontinuously close to $R = 0.1$ pc. The sense of this discontinuity, however, is the reverse of that in Fig. 5, whilst its size is ~ 3 times greater.

Three final points are worth making. The first of these is that nebular filling factors ε are usually assessed through comparison of root mean square densities n_e (rms) and forbidden line estimates of density $n_e(FL)$ (e.g. Fig. 2), whence $\varepsilon = (n_e(\mathrm{rms})/n_e(FL))^2$. Such an analysis, in the present case, would therefore imply a discontinuity in ε close to $R = 0.1$ pc.

In reality, it is by no means clear that responsibility for all of the variation in Fig. 2 can be laid at the door of ε alone; it is probable that much of the density anomaly arises from structural differences between the [S II] and H I emission zones. It is apparent, therefore, that the evaluation of ε using such procedures may lead to considerable errors.

The second point concerns the dispersion in data about the mean trends $n_e(R)$ illustrated in Figs. 2 and 5. When the contributions of parametric errors, differences in nebular structures, and possible variations in density structure (see Sect. 4) are stripped out, it is clear that the residual dispersion is likely to be considerably less. It would appear, in brief, that variations in $n_e(R)$ arising from differing nebular masses and evolutionary trends are relatively low; a feature which presumably has its origin in an initial small progenitor mass range (e.g. Stasinska et al. 1997).

Finally, the trend of n_e (rms) with R (Fig. 5) suggests that the calibration nebulae are reasonably well ordered with respect to radius. It is therefore improbable that the trends in Fig. 2 can be attributed to errors in Dθ alone; that sources having $R > 0.1$ pc are "scattered" into this regime through uncertainties in D and θ. Similarly, we observe no dependency between the differing density trends in Fig. 2 and source morphology. Thus, for instance, bipolar nebulae account for $\sim 10\%$ of nebulae having $R < 0.1$ pc, and $\sim 15\%$ with $R > 0.1$ pc; a difference which is insignificant given the small sample size.

4. Modelling of the [S II] emission zone

The physical origins of the variations in Fig. 2 and Fig. 4 are difficult to comprehend in terms of current models of nebular expansion. Nevertheless, some understanding of the structural origins of this change may perhaps be sought as follows.

Initially, for instance, one might be inclined to suggest that the [S II] emission derives from two mass components; one (component I) with lower density, associated with ionisation stratification of the primary shell structure; the other (higher density) component II arising perhaps from shocks, or at the surfaces of neutral and/or dense inclusions. As the nebulae pass from radiation to density-bound states, the intensity of component I is reduced, and the higher density component predominates. As attractive as this may seem, however, it fails to account for the apparent *increase* in [S II]/Hβ line ratios in nebulae having $R > 0.1$ pc.

Such an increase may however arise through one of at least two further mechanisms. Thus, it is possible that a precipitous reduction in the central star ionising flux may lead to increased low-excitation line strengths, as described by Stasinska (1989), although in the absence of appreciable (and unrealistic) radial density gradients within the primary shells, it is difficult to

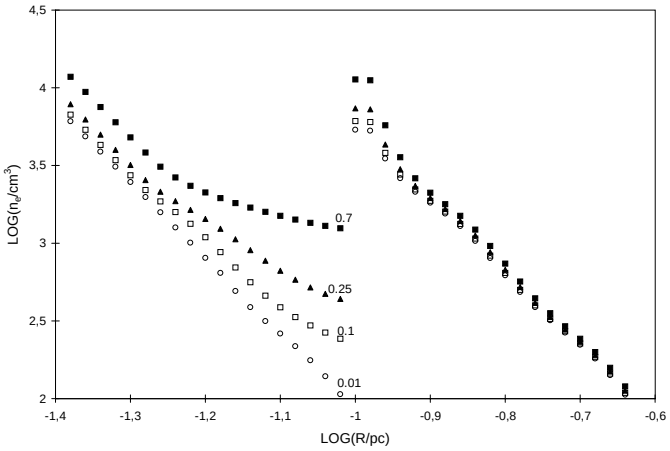

Fig. 6. Two component modelling of the density variation in Fig. 2, where we include solutions for various values of α (see text for details). Note that all of the primary features of the observed variation can be replicated if we assume that one [S II] emission component (component II) has density $\sim 10^2$ greater than the other (component I), and that the [S II] flux from component II increases by an order of magnitude close to $R = 0.1$ pc

see how this could account for the density discontinuity noted above. Alternatively, it is possible that the density and intensity discontinuities are intimately related, one variation leading automatically to the other.

To see how this might arise, we shall assume that component II has an intensity $I_2 = \alpha I_1$ for $R \leq 0.1$ pc, where I_1 is the (invariant) intensity of [S II] emission from component I, and α is a constant. We shall also assume (following Fig. 4) that the intensity of the two components combined ($I_1 + I_2$) increases by a factor 5 in crossing the optically thin/thick interface (see Sect. 3), and that all of this change arises from an increase in intensity of component II.

Under these circumstances, it can be shown that $I_2(R > 0.1\,\mathrm{pc}) = (4 + 5\alpha)I_1$.

For simplicity, if we now take the density variation of component II to be $n_2 = n_{20}R^{\beta}$, and of component I to be $n_1 = n_{10}R^{\beta}$ (that is, the radial gradients are the same), then for $\beta = 5$ and $n_{20}/n_{10} = 10^2$ we find that the combination of both components would lead to the apparent trends in Fig. 6; where we have illustrated the radial changes in density anticipated for several values of α. In the absence of information concerning the origins of zones I and II, we shall also assume electron temperatures $T_e(I) \approx T_e(II)$. If, as will be suggested later, zone II arises from shocking of the primary shell, then it is possible that $T_e(II)$ may differ significantly from $T_e(I)$. Such a difference would be unlikely to affect the qualitative conclusions of this analysis, however.

It is clear, from Fig. 6, that most if not all of the characteristics in Fig. 2 are adequately explained through such a model. In particular, the order of magnitude increase in [S II] emission for the denser gas component would explain the apparent discontinuity in densities where $R = 0.1$ pc; and (providing α is modest and of order 0.3), the slight difference in radial density gradients between optically thick and thin nebulae. The correlation between n_e and R for larger nebulae would be expected to be high, providing only that the increase in emission for component II is appreciable (and of course, that the range of differing PN types is not too great; see the discussion in Sect. 3). On the other hand, the variation of $n_e(R)$ for smaller nebulae is sensitively dependent upon α, and the variation of this parameter may explain the lower correlation between n_e and R for radiation bound sources (Fig. 2).

Finally, the model accommodates, quite nicely, the differing discontinuities noted in Figs. 2 and 4; one discontinuity leading naturally to the other.

It is interesting to note that Phillips & Guzman (1998) have suggested that an appreciable proportion of [S II] emission may arise from shocks. The present work reinforces this conclusion, in suggesting that the [S II] emission zone is far from being either simple or uniform. It appears, rather, that much of the [S II] emission may arise from dense post-shock cooling zones, associated perhaps with the exterior shocks to be discussed below.

Finally, it is pertinent to ask why [S II] emission should increase so precipitously for optically thin sources, and why this amplification should be associated with component II.

One possible avenue to understanding such changes may be found in the 3 winds modelling of Schmidt-Voigt & Köppen (1987a) and Marten & Schönberner (1991), where a superwind flow is presumed to be interacting with both an interior stellar wind, and external AGB outflow. In particular, exterior shell velocities for such models appear to be a strongly variable function of radius. Where the ionisation front breaks through the superwind envelope, then velocities would be expected to increase appreciably as the shell accelerates into the AGB envelope; the degree of acceleration depending upon the density contrast between superwind and AGB flows.

Shocking of the AGB envelope may, under these circumstances, be expected to lead to a compressed post-shock zone, together with appreciable enhancement of [S II] and other low excitation transitions. It is therefore possible that the observed discontinuities have an origin in a kinematic "jump" close to $R = 0.1$ pc; the resulting enhanced shock leading to increases in emission from the high density, post-shock cooling zone (component II).

There are however two problems with such an hypothesis. In the first place, and following the analysis of Phillips & Guzman (1998), it can be shown that for a spherical shock enveloping a nebula with mean density n_e then

$$\frac{I_s\,([\mathrm{S\,II}])}{I_r\,(\mathrm{H}\beta)} = 0.81\frac{\{I_s\,([\mathrm{S\,II}]/I_s\,(\mathrm{H}\beta))\}\,\{R/\mathrm{pc}\}^2\,U\,(V_s)}{\{M/M_{\odot}\}} \times \left\{\frac{^{pr}n_e}{n_e}\right\}$$

where I_s ([S II]) is the [S II] flux emerging from the shock; I_r (Hβ) is the radiatively excited Hβ flux (deriving from the primary ionised mass); M is the nebular mass; $\mu(= 1.36)$ is the mean atomic weight per H atom; $F_s(\mathrm{H}\beta) = U(V_s)(^{pr}n_e/10^2\ \mathrm{cm}^{-2})$ is the Hβ flux through the shock front in units of 10^{-4} ergs cm^{-2} s^{-1}, and $^{pr}n_e$ is the pre-shock den-

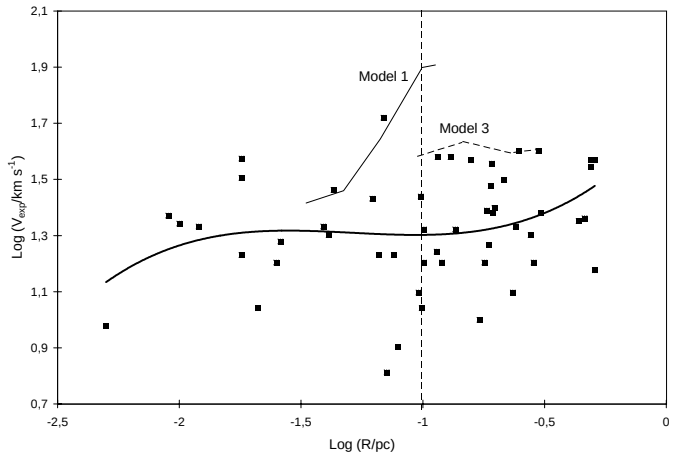

Fig. 7. Variation of observed PN expansion velocities as a function of radius. Also shown are velocities anticipated for two of the models of Schmidt-Voigt & Köppen (1987a)

sity. Where $I_s(\mathrm{H}\beta) \ll I_r(\mathrm{H}\beta)$ and I_r ([S II]) $\leq I_s(\mathrm{H}\beta)$, then such an expression also represents a reasonable approximation to observed line ratios where nebulae are appreciably shocked.

Adopting values $M = 0.1 M_\odot$, $R = 0.1$ pc, assuming that ${}^{pr}n_e = n_e$, and employing the planar shock estimates for $U(V_s)$ and $I_s([\mathrm{S\,II}])/I_s(\mathrm{H}\beta)$ from Hartigan et al. (1987) then yields values $I_s([\mathrm{S\,II}])/I_r(\mathrm{H}\beta) \sim 0.027 \rightarrow 0.067$ for $V_s = 30 \rightarrow 80\,\mathrm{km\,s^{-1}}$. This flux ratio is significantly less than the observed value $F_s([\mathrm{S\,II}])/F_r(\mathrm{H}\beta) \sim 0.32$ for nebulae having $R > 0.1$ pc, and the disparity would increase still further where more realistic values of ${}^{pr}n_e/n_e$ are employed. It appears, therefore, that such shocks would be unlikely to enhance [S II]/Hβ line ratios by the appropriate amount.

The second problem relates to the presence or otherwise of the kinematic jumps. One way of checking this might, for instance, be to determine the variation of observed [S II] velocities close to the $R = 0.1$ pc transition boundary.

Sadly, the number of available [S II] shell expansion measures is rather limited, and the best we can do is to investigate the variation of V_{exp} using the [N II] $\lambda\lambda$ 6548+6584 Å lines; transitions which are associated with similar peripheral nebular emission zones.

The corresponding variation of V_{exp} ([N II]) is illustrated in Fig. 7, where we have used the Catalogue of expansion velocities due to Weinberger (1989), and the nebular radii of CKS. We have also illustrated models 1 (solid line) and 3 (dashed line) of Schmidt-Voigt & Köppen (1987a), corresponding to respective superwind/AGB density contrasts of 500 and 17, together with a third order least squares polynomial regression curve (solid curve).

It is plain, from this, that there is precious little evidence for velocity changes close to $R \sim 0.1$ pc; and certainly nothing to support the velocity variations of model 1. It therefore seems that either the [N II] velocities are not accurately reflecting peripheral shell velocities; that the assumed velocity jump is small (< 0.15 dex) or non-existent; or finally, that any increase in velocities is being smeared through errors in R.

Taken as a whole, it would therefore seem that the acceleration of the envelope postulated above is unlikely to explain the unusual evolutionary characteristics of the [S II] $\lambda\lambda$ 6717+6730 Å doublet, and further analysis of this question is urgently required.

5. Nebular distances

Although the radial density gradients in Fig. 2 may be somewhat dependent upon errors in n_e and (in particular) θ, it is also evident that the correlation between $D\theta$ and n_e is reasonably high, and essentially unaffected by uncertainties in IS extinction. Similarly, given that D is directly proportional to θ, and only weakly dependent upon n_e, it follows that Eqs. 1 and 2 should enable estimates of distance to a reasonable level of accuracy; typical errors in log $D\theta$ are unlikely to exceed $\Delta \log D\theta \sim 0.1$ for $R > 0.1$ pc, and $\Delta \log D\theta \sim 0.2$ for $R \leq 0.1$ pc. The primary problem is to evaluate whether the nebula is optically thin or thick to ionising radiation; that is, on which of the sequences the source belongs.

For the latter purpose, we have used the trend for F(5 GHz) fluxes determined by Zhang (1995) to define a surface brightness $F(5\,\mathrm{GHz})/\theta^2 < 1.42\,10^{-3}$ Jy arcsec^{-2} for $R > 0.1$ pc (that is, the brightness temperature of the source is < 23.71 K). A very similar limit is obtained from the analysis of Van de Steene & Zijlstra (1994). The observed radio surface brightness may therefore be employed as a species of sorting code. Similarly, we have also employed the [S II] data base of Kaler et al. (1997) to evaluate densities for 262 sources.

The resulting mean densities are given in Table 3. In order to determine these densities (and to assure reasonable compatibility with the densities of Table 1), we have used similar [S II] collision strengths and transition probabilities to those employed by Stanghellini & Kaler (1989). Nebular temperatures have been taken from Cahn et al. (1992); on the few occasions where values $t = T_e/10^4$ K are not available, we have employed a mean value $t = 1.12$ K. Although these estimates of t are often different from those assumed by Stanghellini & Kaler (1989) (sometimes appreciably so), the change in the estimates of $\log n_e$ is modest. Thus, from a comparison of densities obtained here (n_e (present)) and by Stanghellini & Kaler (1989) ($n_e(SK)$), we find that $\langle \log n_e \text{ (present)} - \log n_e(SK) \rangle = 0.018 \pm 0.024$ for the 67 sources common to both lists; that is, there is no significant difference in density.

Finally, values of radio flux and nebular size are taken from previous compilations by Aaquist & Kwok (1990), Milne (1979), Milne & Aller (1975), and Zijlstra et al. (1989) (although see also Pottasch & Zijlstra (1994) for a discussion of corrections to the latter reference).

The nebular distances, radii, and densities evaluated here are summarised in Table 3. A comparison between these values of D, and those of Daub (1982), Cahn et al. (1992), Van de Steene & Zijlstra (1994) and Zhang (1995) is further provided in Fig. 8. Several features are noteworthy. First, there is a reasonable correlation between present values of distance and the comparative estimates, although the range of scatter increases fan-like as D

Table 3. Planetary nebulae distances

Source	PK No.	T_e 10^4 K	Log n_e	Sample	Radius arcsec	F(5 GHz) jy	Distance kpc	Radius pc
A 1	119+061	1.16	2.66	1	23.50	0.006	2.08	0.236
A 11	196-121	1.02	2.71	1	16.00	0.010	2.99	0.232
A13	204-081	1.02	3.20	1	76.30	0.008	0.50	0.185
A30	208-331	1.12	3.41	1	63.50	0.002	0.55	0.169
A41	009+101	1.12	2.63	1	9.20	0.005	5.38	0.240
A59	053+031	1.02	2.07	1	43.00	0.018	1.49	0.311
A71	085+041	1.16	2.34	1	79.00	0.083	0.72	0.275
A 82	114-041	1.06	2.71	1	40.50	0.005	1.18	0.233
Ap 1-12	003-047	1.02	3.76	1	6.00	0.019	1.24	0.036
Bl M	001-011	1.02	2.63	1	2.30	0.017	6.69	0.075
BV 1	119+001	1.41	2.51	2	20.80	0.018	2.52	0.254
Cn 1-5	002-091	1.02	3.65	3	3.50	0.044	2.28	0.039
Cn 2-1	356-041	1.02	4.01	2	1.28	0.052	4.93	0.030
Cn 3-1	038+121	2.15	3.86	3	2.40	0.067	2.89	0.034
Fg 1	290+071	1.02	2.60	2	10.80	0.055	1.45	0.076
Ha 1-2	347+051	1.02	3.98	1	0.40	0.062	16.01	0.031
Ha 1-15	001+052	1.02	3.12	1	2.20	0.013	5.10	0.054
Ha 1-19	358+034	1.02	3.08	1	0.70	0.026	16.39	0.056
Ha 1-20	358+034	1.02	3.97	1	1.40	0.044	4.60	0.031
Ha 1-23	357+011	1.02	3.70	2	1.40	0.035	5.50	0.037
Ha 1-24	004+062	1.02	4.03	1	4.30	0.015	1.45	0.030
Ha 1-27	005+041	1.02	3.44	1	2.60	0.018	3.51	0.044
Ha 1-33	355-031	1.02	3.47	1	1.40	0.012	6.38	0.043
Ha 1-35	355-033	1.02	4.31	2	1.00	0.089	5.20	0.025
Ha 1-36	353-041	1.02	4.31	1	0.80	0.081	6.50	0.025
Ha 1-39	356-033	1.02	3.78	1	0.90	0.014	8.12	0.035
Ha 1-40	359-023	1.02	4.24	1	1.90	0.063	2.86	0.026
Ha 1-42	357-041	1.02	3.39	1	2.90	0.040	3.25	0.046
Ha 1-43	357-043	1.02	3.49	1	1.50	0.006	5.86	0.043
Ha 1-46	358-041	1.02	4.03	1	0.60	0.043	10.39	0.030
Ha 1-50	358-053	1.02	3.60	1	0.70	0.031	11.72	0.040
Ha 1-56	001-042	1.02	3.71	1	1.50	0.008	5.10	0.037
Ha 1-59	003-043	1.47	3.09	2	3.00	0.004	3.81	0.055
Ha 1-65	007-041	1.02	3.99	2	2.60	0.017	2.46	0.031
Ha 1-66	007-061	1.02	3.20	2	3.30	0.006	3.21	0.051
Ha 1-67	009-041	1.02	3.24	1	3.00	0.011	3.46	0.050
Ha 2-1	350+041	1.02	3.60	2	2.80	0.065	2.93	0.040
Ha 2-10	358+032	1.02	3.19	1	1.00	0.020	10.71	0.052
Ha 2-15	003+051	1.02	3.18	1	1.70	0.002	6.33	0.052
Ha 2-16	005+052	1.02	2.23	1	8.40	0.004	7.09	0.289
Ha 2-17	003+031	1.02	3.22	1	1.80	0.010	5.85	0.051
Ha 2-20	002+011	1.02	3.89	1	1.90	0.016	3.58	0.033
Ha 2-24	004+011	1.02	2.46	1	2.30	0.013	7.44	0.083
Ha 2-25	004+021	1.02	4.41	1	2.20	0.004	2.21	0.024
Ha 2-43	003-049	1.02	4.03	1	4.50	0.026	1.38	0.030
Hb 4	003+021	1.06	3.78	2	3.00	0.166	2.44	0.035
Hb 5	359-001	1.38	3.87	2	10.00	0.621	0.69	0.033
Hb 6	007+011	1.10	3.42	2	2.75	0.240	3.35	0.045
Hb 12	11-021	1.02	3.52	3	0.38	0.080	23.05	0.042
He 1-5	060-071	1.02	2.35	1	18.00	0.005	3.13	0.273
He 1-6	065-051	1.02	1.65	1	11.20	0.020	6.90	0.375
He 2-5	283+031	1.02	3.87	1	5.90	0.029	1.17	0.033
He 2-29	275-022	1.02	2.85	1	7.00	0.024	1.91	0.065
He 2-37	274+031	1.02	2.32	1	11.50	0.023	4.96	0.277
He 2-51	288-051	1.02	2.77	1	4.50	0.057	3.12	0.068

Table 3. (continued)

Source	PK No.	T_e 10^4 K	Log n_e	Sample	Radius arcsec	F(5 GHz) jy	Distance kpc	Radius pc
He 2-86	300-021	1.02	4.22	1	1.80	0.125	3.06	0.027
He 2-99	309-041	1.02	3.50	2	8.50	0.018	3.91	0.161
He 2-111	315-001	1.90	3.12	3	6.00	0.073	1.87	0.054
He 2-112	319+061	1.02	3.31	2	7.30	0.082	1.36	0.048
He 2-115	321+021	1.02	4.36	1	1.50	0.156	3.36	0.024
He 2-119	317-051	1.02	2.60	1	25.70	0.094	1.96	0.244
He 2-123	323+021	1.02	3.64	1	2.30	0.110	3.47	0.039
He 2-131	315-131	1.02	3.85	2	3.00	0.335	2.33	0.034
He 2-138	320-091	1.02	3.47	1	3.50	0.076	2.55	0.043
He 2-140	327-012	1.02	4.03	1	1.30	0.080	4.79	0.030
He 2-153	330-021	1.02	3.09	1	6.50	0.001	6.17	0.194
He 2-157	331-021	1.02	4.20	1	1.50	0.030	3.72	0.027
He 2-175	345+061	1.02	3.55	2	3.30	0.027	2.57	0.041
He 2-250	000+031	1.12	3.06	2	2.80	0.015	4.16	0.056
He 2-260	008+061	1.02	3.39	1	0.50	0.013	18.87	0.046
He 2-459	068-021	1.02	3.71	1	0.83	0.055	9.28	0.037
Hf 2-1	335-041	1.02	2.86	1	4.70	0.009	2.82	0.064
Hu 1-1	119-061	1.21	3.23	4	3.75	0.023	2.79	0.051
Hu 1-2	086-081	1.71	3.68	8	3.30	0.293	2.36	0.038
Hu 2-1	051+091	0.96	3.61	5	1.20	0.103	6.80	0.040
IC 351	159-151	1.20	3.28	2	3.50	0.035	2.89	0.049
IC 1297	358-211	1.08	3.44	2	3.50	0.069	2.61	0.044
IC 1454	117+181	1.07	2.42	2	17.00	0.001	3.21	0.264
IC 1747	130+011	1.01	3.60	3	6.45	0.128	1.27	0.040
IC 2003	161-141	1.21	3.76	5	3.88	0.047	1.91	0.036
IC 2149	166+101	1.03	3.65	4	4.43	0.309	1.80	0.039
IC 2165	221-121	1.39	3.65	4	3.93	0.202	2.03	0.039
IC 2553	285-051	1.01	3.94	1	4.45	0.137	1.48	0.032
IC 4191	304-341	1.05	3.81	1	7.00	0.170	1.03	0.035
IC 4406	319+151	1.05	3.13	1	13.63	0.110	0.81	0.054
IC 4593	025+401	1.12	3.21	2	6.40	0.092	1.66	0.051
IC 4634	000+121	1.12	4.12	2	3.48	0.122	1.69	0.028
IC 4673	003-023	1.40	2.99	1	7.40	0.060	1.64	0.059
IC 4732	010-061	1.48	4.27	1	2.25	0.037	2.37	0.026
IC 4776	002-131	0.86	4.08	1	3.50	0.065	1.72	0.029
IC 4846	027-091	1.00	3.58	2	1.28	0.059	6.54	0.040
IC 5117	089-051	1.16	3.81	2	0.70	0.232	10.23	0.035
IC 5148		1.16	3.38	1	60.00	0.028	0.59	0.171
IC 5217	100-051	1.12	3.65	4	3.40	0.048	2.33	0.038
J 320	190-171	1.26	3.24	4	3.58	0.021	2.90	0.050
J 900	194+021	1.21	3.70	4	3.00	0.110	2.57	0.037
K 1-22	283+251	1.02	3.33	1	90.50	0.012	0.40	0.175
K 3-60	098+041	1.02	3.59	1	0.98	0.043	8.47	0.040
K 3-61	096+021	1.02	2.75	2	3.00	0.014	4.75	0.069
K 3-66	167-091	1.02	3.80	1	1.08	0.018	6.72	0.035
K 3-67	165-061	1.02	3.91	2	4.30	0.005	6.41	0.134
K 3-77	078+001	1.02	3.12	1	3.80	0.027	2.94	0.054
K 3-86	106-041	1.51	1.74	1	4.70	0.001	15.82	0.360
K 3-92	130-031	0.99	2.11	1	6.50	0.002	9.67	0.305
K 4-45	096+001	1.02	3.11	2	25.75	0.005	1.54	0.196
Lo 4	274+091	2.05	2.95	1	24.00	0.000	1.78	0.207
M 1-1	130-111	1.50	3.75	2	2.75	0.010	2.72	0.036
M 1-4	147-021	1.28	3.83	4	2.50	0.084	2.83	0.034
M 1-5	184-021	0.91	3.29	2	1.13	0.071	8.94	0.049
M 1-8	210+011	1.20	2.62	3	4.00	0.023	3.86	0.075

Table 3. (continued)

Source	PK No.	T_e 10^4 K	Log n_e	Sample	Radius arcsec	F(5 GHz) jy	Distance kpc	Radius pc
M 1-12	235-031	1.02	3.90	3	0.90	0.044	7.53	0.033
M 1-13	232-011	1.02	3.03	2	5.00	0.015	2.37	0.057
M 1-14	235-011	1.05	3.70	1	2.38	0.056	3.24	0.037
M 1-16	226+051	1.12	2.89	1	1.65	0.028	7.88	0.063
M 1-17	228+051	1.03	3.71	2	1.33	0.017	5.79	0.037
M 1-20	006+081	1.02	4.03	1	1.90	0.051	3.28	0.030
M 1-22	007-071	1.02	3.22	2	3.00	0.330	3.50	0.051
M 1-25	004+041	1.02	3.85	2	1.95	0.055	3.57	0.034
M 1-27	356-022	1.02	3.73	1	4.00	0.063	1.89	0.037
M 1-28	006+032	1.02	2.63	1	7.40	0.020	2.08	0.075
M 1-29	359-011	1.02	3.67	1	3.80	0.102	2.07	0.038
M 1-30	355-042	1.02	3.68	2	1.90	0.031	4.10	0.038
M 1-31	006+025	1.02	3.74	1	3.50	0.057	2.15	0.036
M 1-33	013+041	1.02	3.41	1	1.90	0.060	4.87	0.045
M 1-34	357-051	1.02	3.02	2	5.60	0.015	2.13	0.058
M 1-35	003-021	1.11	3.71	2	2.40	0.057	3.18	0.037
M 1-37	002+031	1.12	3.66	1	1.35	0.015	5.83	0.038
M 1-38	002-035	1.02	4.17	2	1.80	0.045	3.16	0.028
M 1-39	015+031	1.02	3.27	1	2.00	0.100	5.09	0.049
M 1-40	008-011	1.24	4.01	1	2.33	0.208	2.71	0.031
M 1-41	006-021	1.09	2.76	3	38.00	0.350	1.23	0.226
M 1-42	002-042	1.10	3.31	3	4.30	0.024	2.30	0.048
M 1-44	004-042	1.02	3.31	2	2.00	0.009	4.97	0.048
M 1-46	016-011	1.02	3.57	1	5.75	0.086	1.46	0.041
M 1-50	014-041	1.02	3.55	1	2.80	0.050	3.03	0.041
M 1-51	021-011	1.02	3.53	2	7.50	0.319	1.15	0.042
M 1-54	016-041	1.02	3.29	1	6.50	0.038	1.54	0.049
M 1-56	016-042	1.02	3.49	1	0.70	0.021	12.57	0.043
M 1-60	019-041	1.02	3.91	1	1.30	0.052	5.17	0.033
M 1-61	019-051	1.02	3.87	2	0.90	0.097	7.69	0.034
M 1-65	043+031	1.02	3.45	1	1.90	0.022	4.77	0.044
M 1-67	050+031	1.02	3.18	1	60.20	0.250	0.64	0.187
M 1-72	054-021	1.02	3.30	1	0.35	0.026	28.51	0.048
M 1-74	052-041	0.93	4.09	4	0.50	0.031	11.99	0.029
M 1-75	068-001	1.02	3.16	3	7.00	0.026	1.56	0.053
M 1-78	093+011	1.02	3.45	3	3.20	1.104	2.82	0.044
M 1-79	093-021	1.04	2.47	1	15.00	0.019	3.55	0.258
M 1-80	107-021	1.02	3.07	4	4.00	0.025	2.90	0.056
M 2-4	349+041	1.02	3.61	1	2.63	0.032	3.10	0.039
M 2-5	351+051	1.02	3.31	2	2.28	0.012	4.36	0.048
M 2-10	354+041	1.02	3.47	3	1.10	0.009	8.10	0.043
M 2-11	356+041	1.02	3.32	2	1.38	0.021	7.17	0.048
M 2-13	011+111	1.02	3.64	1	0.78	0.013	10.29	0.039
M 2-15	011-061	1.09	3.30	1	2.90	0.013	3.45	0.048
M 2-16	357-032	1.02	3.59	1	2.70	0.025	3.06	0.040
M 2-18	357-034	1.02	3.76	1	0.78	0.017	9.57	0.036
M 2-19	000-015	1.02	3.28	2	2.50	0.014	4.04	0.049
M 2-21	000-024	1.19	3.39	2	1.50	0.023	6.25	0.045
M 2-22	357-042	1.02	3.35	1	2.55	0.011	3.77	0.047
M 2-23	002-024	1.02	4.18	3	4.40	0.070	1.29	0.027
M 2-24	356-052	1.02	3.15	1	3.70	0.003	10.56	0.189
M 2-26	003-022	1.02	2.97	1	4.00	0.005	10.62	0.206
M 2-27	359-042	1.02	3.93	1	1.08	0.029	6.15	0.032
M 2-28	000-041	1.02	3.23	1	2.35	0.010	4.45	0.051
M 2-29	004-031	1.02	3.34	2	2.28	0.008	4.26	0.047

Table 3. (continued)

Source	PK No.	T_e 10^4 K	Log n_e	Sample	Radius arcsec	F(5 GHz) jy	Distance kpc	Radius pc
M 2-30	003-048	1.02	3.20	3	1.88	0.014	5.69	0.052
M 2-33	002-061	1.02	3.05	2	1.90	0.022	6.17	0.057
M 2-36	003-061	1.02	3.55	1	3.45	0.025	2.46	0.041
M 2-38	005-051	1.02	3.46	1	4.00	0.008	2.24	0.044
M 2-39	008-041	1.02	3.24	1	1.60	0.008	6.49	0.050
M 2-42	008-042	1.02	3.22	2	2.00	0.014	5.25	0.051
M 2-44	028+011	1.02	2.54	1	4.00	0.054	4.06	0.079
M 2-46	024-021	1.02	3.66	1	2.35	0.003	3.36	0.038
M 2-49	095-021	1.02	3.30	2	1.18	0.074	8.46	0.048
M 2-51	103+001	1.04	2.47	1	19.60	0.041	2.72	0.259
M 2-55	116+081	1.02	2.71	2	20.00	0.019	2.39	0.232
M 3-1	242-111	1.13	3.52	2	5.55	0.024	1.56	0.042
M 3-6	254+051	1.02	4.03	1	4.10	0.091	1.52	0.030
M 3-10	358+031	1.02	3.51	1	1.60	0.029	5.42	0.042
M 3-11	005+061	1.02	2.70	1	3.55	0.011	4.15	0.071
M 3-12	005+051	1.02	3.09	1	3.23	0.015	3.54	0.055
M 3-14	355-021	1.02	3.56	1	2.50	0.030	3.38	0.041
M 3-16	358-022	1.02	3.19	1	3.30	0.017	3.24	0.052
M 3-17	358-031	1.02	4.48	1	1.48	0.012	3.15	0.023
M 3-20	002-022	1.02	3.71	1	2.00	0.040	3.82	0.037
M 3-21	355-061	1.02	4.03	2	2.50	0.030	2.49	0.030
M 3-23	000-042	1.02	2.46	1	6.00	0.028	2.85	0.083
M 3-30	017-041	1.16	2.25	1	9.80	0.007	6.02	0.286
M 3-33	009-101	1.02	3.48	1	3.00	0.008	2.96	0.043
M 3-35	071-021	1.02	3.86	2	0.75	0.150	9.26	0.034
M 3-37	359+061	1.02	2.68	1	1.10	0.005	13.51	0.072
M 3-38	356+042	1.02	4.03	1	0.90	0.021	6.92	0.030
M 3-40	358+052	1.02	3.03	1	1.28	0.018	9.33	0.058
M 3-41	357+032	1.02	3.73	1	2.10	0.075	3.61	0.037
M 3-42	357+034	1.02	3.07	1	4.50	0.006	9.02	0.197
M 3-43	000-011	1.02	3.19	1	1.90	0.027	5.63	0.052
M 4-3	357+071	1.12	3.50	1	0.65	0.028	13.48	0.042
M 4-18	146+071	1.02	3.32	2	1.90	0.019	5.18	0.048
Me 1-1	052-022	1.02	4.32	1	2.38	0.043	2.18	0.025
Me 2-1	342+271	1.24	3.34	3	3.25	0.024	2.99	0.047
Me 2-2	100-081	1.08	3.36	1	0.65	0.025	14.71	0.046
MyCn 18	307-041	1.02	4.40	1	4.65	0.106	1.05	0.024
Mz 2	329-022	1.02	3.75	1	11.45	0.075	0.65	0.036
Mz 3	331-011	1.02	3.79	3	12.70	0.649	0.57	0.035
NGC 40	120+091	1.10	3.33	4	18.20	0.460	0.54	0.047
NGC 650	130-10	1.07	2.58	4	59.60	0.110	0.85	0.245
NGC 1501	144+061	1.51	3.27	1	26.45	0.224	1.40	0.179
NGC 2022	196-101	1.49	3.32	2	9.78	0.091	1.01	0.048
NGC 2371	189+19	0.69	2.97	5	24.40	0.090	1.74	0.206
NGC 2438	231+042	1.09	2.73	1	37.60	0.073	1.26	0.229
NGC 2867	278-051	1.16	3.47	1	7.80	0.299	1.15	0.043
NGC 2899	277-031	1.49	2.45	2	45.00	0.086	1.20	0.261
NGC 3195	296-201	1.02	2.44	1	19.85	0.035	2.72	0.262
NGC 3587	148+571	1.09	2.33	1	92.50	0.091	0.62	0.276
NGC 5189	307-031	1.27	2.85	4	70.00	0.507	0.64	0.218
NGC 5882	327+101	0.93	4.46	1	7.00	0.334	0.67	0.023
NGC 6072	342+101	1.14	3.23	1	35.00	0.181	1.08	0.183
NGC 6153	341+051	1.11	3.86	2	12.00	0.632	0.58	0.034
NGC 6210	043+371	0.97	3.46	4	8.10	0.256	1.11	0.043
NGC 6309	009+141	1.13	3.48	2	6.90	0.167	1.29	0.043

Table 3. (continued)

Source	PK No.	T_e 10^4 K	Log n_e	Sample	Radius arcsec	F(5 GHz) jy	Distance kpc	Radius pc
NGC 6337	349-011	1.02	2.64	1	23.50	0.143	2.09	0.238
NGC 6369	002+051	1.25	3.52	1	14.15	2.002	0.61	0.042
NGC 6537	010+001	1.57	3.43	1	2.85	0.624	3.22	0.044
NGC 6543	096+291	0.81	3.26	11	9.70	0.899	1.05	0.050
NGC 6563	358-071	1.06	2.63	1	22.05	0.070	2.24	0.240
NGC6620	005-061	1.15	3.43	3	2.50	0.010	3.67	0.044
NGC6644	008-072	1.26	4.05	3	1.43	0.098	4.31	0.030
NGC6751	029-051	1.03	3.22	9	10.50	0.063	1.00	0.051
NGC6765	062+091	1.17	3.05	1	19.00	0.018	2.15	0.198
NGC6778	034-061	0.80	2.97	4	7.95	0.055	1.55	0.060
NGC 6781	041-021	1.00	2.67	4	53.00	0.323	0.92	0.236
NGC6790	037-061	1.28	4.02	3	1.70	0.272	3.68	0.030
NGC6807	042-061	1.69	4.46	1	0.70	0.027	6.74	0.023
NGC6818	025-171	1.28	3.27	3	9.25	0.304	1.10	0.049
NGC6826	083+121	1.12	3.20	12	12.70	0.404	0.84	0.052
NGC6881	074+021	1.14	4.16	2	1.90	0.124	3.01	0.028
NGC6894	069-021	1.02	2.46	3	24.75	0.061	2.16	0.260
NGC6905	061-091	1.21	3.02	2	21.85	0.062	1.89	0.201
NGC7048	088-011	1.26	2.09	1	31.25	0.037	2.03	0.307
NGC7293	036-571	1.10	2.27	13	351.00	1.292	0.17	0.284
PB 6	278+051	1.44	3.40	1	5.50	0.030	1.69	0.045
PC 12	000+171	1.02	3.78	2	0.90	0.019	8.13	0.035
PC 14	336-061	1.02	3.44	1	3.50	0.030	2.60	0.044
Pe 1-5	333+011	1.02	3.71	2	5.50	0.233	1.39	0.037
Pe 1-11	358-051	1.02	2.51	1	4.50	0.008	3.69	0.080
Pe 1-17	024-031	1.02	3.29	1	3.25	0.006	3.09	0.049
Pe 2-12	002-023	1.02	2.70	1	2.50	0.002	19.16	0.232
Sh 1-89	089-001	1.02	2.58	3	19.00	0.043	2.67	0.246
Sh 2-71	036-011	1.42	2.51	1	53.40	0.066	0.98	0.254
Sh 2-266	195-001	1.02	2.46	1	33.50	0.145	1.59	0.259
Sn 1	013+321	1.00	2.88	1	1.50	0.007	8.74	0.064
Th 2-A	306-001	1.02	3.10	1	11.85	0.060	0.95	0.055
Th 3-10	355+022	1.02	4.02	1	1.00	0.030	6.28	0.030
Th 3-26	358+038	1.02	3.24	1	3.28	0.010	3.17	0.050
Th 4-5	009+041	1.02	3.46	1	3.50	0.016	2.57	0.044
VV 1-2	151+021	1.02	2.63	1	130.00	0.265	0.38	0.240
VV 1-4	197-021	1.02	2.74	2	63.20	0.553	0.75	0.229
Vy 1-1	118-081	1.02	2.25	1	3.05	0.029	6.43	0.095
Vy 1-2	053+241	0.97	3.28	2	2.30	0.012	4.38	0.049
Vy 2-1	007-062	1.02	3.60	1	1.38	0.038	5.97	0.040
Vy 2-3	107-131	1.03	3.45	1	2.30	0.003	3.93	0.044
Ym 29	205+141	1.12	2.29	5	307.50	0.327	0.19	0.281

increases. This trend suggests a typical error in angular radius $\Delta\theta \sim 0.35\theta$. Although Table 2 includes nebulae of all angular sizes, proportionate errors $\Delta\theta/\theta$ increase with decreasing θ. We have therefore excluded from the figures those sources having $\theta < 1$ arcsec.

A second point to note is that the present distances are, in the mean, smaller than those of VdSZ and Zhang, and comparable to those of Daub and CSK. Specifically, and for all of the nebulae in the present sample, we find mean ratios $\langle D(\mathrm{CKS})\rangle \,/\, \langle D(\mathrm{NEW})\rangle = 1.05$; $\langle D(Z)\rangle \,/\, \langle D(\mathrm{NEW})\rangle = 1.27$; $\langle D(\mathrm{VdSZ})\rangle \,/\, \langle D(\mathrm{NEW})\rangle = 1.23$; and $\langle D(\mathrm{Daub})\rangle \,/\, \langle D(\mathrm{NEW})\rangle = 0.91$. If nebulae having $\theta < 1$ arcsec are excluded, then the scale ratios change to $\langle D(\mathrm{CKS})\rangle \,/\, \langle D(\mathrm{NEW})\rangle = 1.28$; $\langle D(Z)\rangle \,/\, \langle D(\mathrm{NEW})\rangle = 1.48$; $\langle D(\mathrm{VdSZ})\rangle \,/\, \langle D(\mathrm{NEW})\rangle = 1.40$; and $\langle D(\mathrm{Daub})\rangle \,/\, \langle D(\mathrm{NEW})\rangle = 0.95$.

It would appear, in brief, that distances derived using this new procedure imply a mean distance scale which is less than

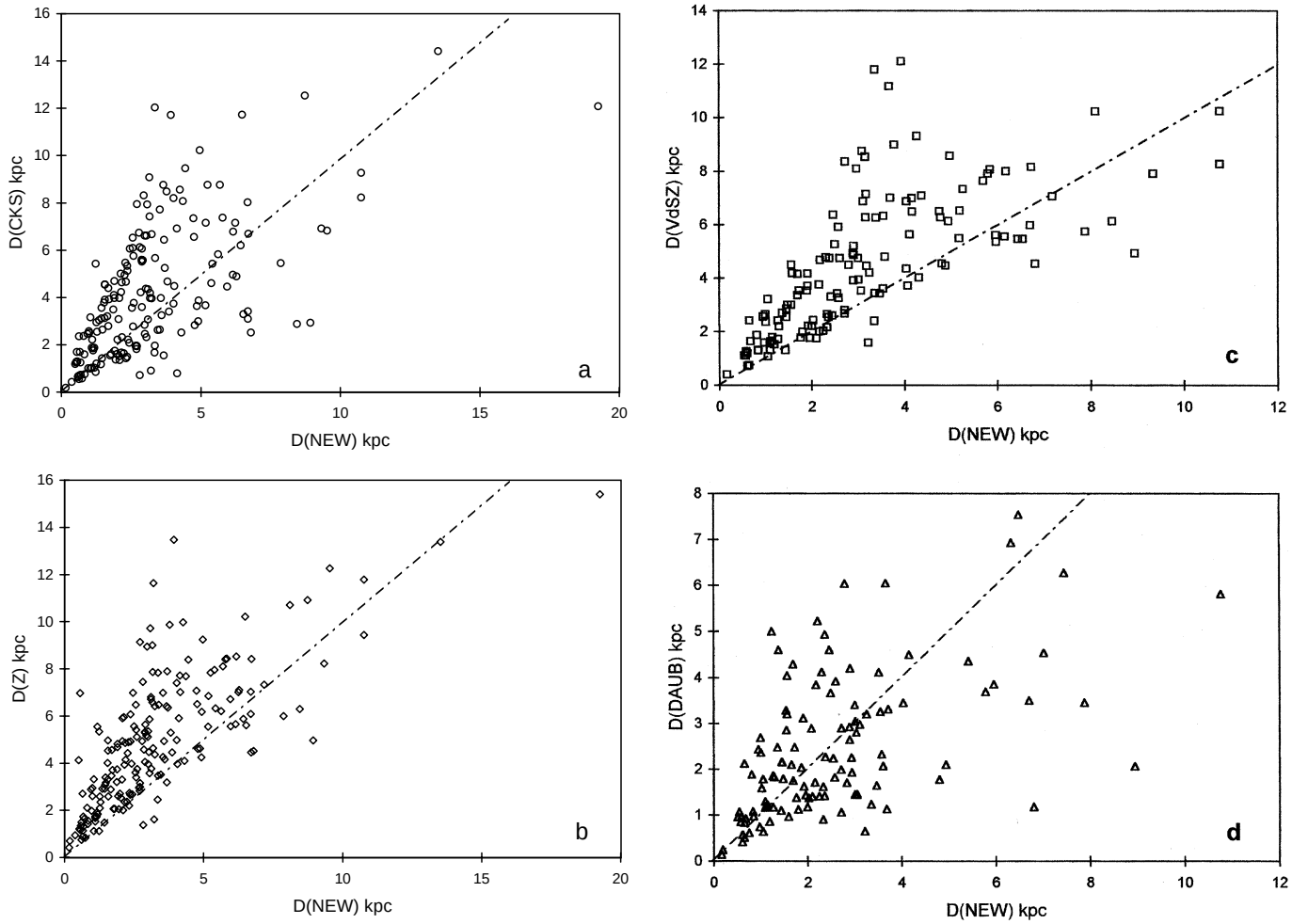

Fig. 8a–d. Comparison of the present values of nebular distance with those evaluated by Cahn et al. (1992; CKS), Zhang (1995; Z), Van de Steene & Zijlstra (1994; VdSZ) and Daub (1982); the diagonal lines would correspond to a one-to-one relation. The distances of VdSZ and Zhang appear, in particular, to be greater than those deduced here

that of most other methods (including those also of Cudworth (1974), Mendez et al. (1988, 1990), Mallik & Peimbert (1988) and Peimbert (1990)), and closely aligned to those of Daub and CKS; although the precise scaling ratios depend upon the ranges of source size θ which are included.

6. Conclusions

We have investigated the radial variation of [S II] electron densities for a sample of 34 nebulae having reasonably well-defined distances. As a result, it is apparent that there is a discontinuous jump in densities of order 1.4 dex close to the transition radius $R = 0.1$ pc. This variation appears also to be associated with an appreciable change in [S II] line intensities.

We believe that such trends may be explicable where there are two components of [S II] emission; one deriving from the primary shell, the other from a region some 10^2 times denser, associated perhaps with shock compression. The intensity of emission from the dense component appears to increase by an order of magnitude as nebulae pass from radiative to density-bound expansion regimes.

Such a variation can, we believe, explain the differing apparent trends in $n_e(R)$; the differing levels of correlation between n_e and R; and the apparent discontinuous change in density between optically thin and thick nebulae. The origins of these density structures, on the other hand, are rather less obvious. In particular, we have noted that the transition from radiative to density-bound phases of expansion may be associated with acceleration of the outer envelope; and that the resulting shocks might plausibly result in similar apparent discontinuities. More detailed analysis, however, suggests that the enhancement in [S II] line strengths is unlikely to be sufficient, whilst [N II] expansion velocities provide little evidence for the required kinematic jumps.

Finally, the deduced density functions are sufficiently well defined to suggest an alternative method for estimating nebular distance. We have, for this purpose, determined electron densities in 262 nebulae using [S II] line ratios deriving from the published literature. The resulting distances appear to be smaller than those of Zhang (1995) and Van de Steene & Zijlstra (1994),

but comparable (in scale) to those of Daub (1982) and Cahn et al. (1992).

Acknowledgements. I would like to express my gratittude to Pablo Ramirez Beraud for his help in tabulating certain of this data.

References

Aaquist A., Kwok S., 1990, A&AS 84, 229
Barker T., 1978, ApJ 219, 914
Barker T., 1984, ApJ 284, 589
Bedogni *R.*, D'Ercole A., 1986, A&A 157, 101
Boffi F.*R.*, Stanghellini L., 1994, A&A 284, 248
Cahn J.H., Kaler J.B., Stanghellini L., 1992. A&AS 94, 399
Cudworth K.M., 1974, AJ 79, 1384
Daub C.T., 1982, ApJ 260, 612
Dufour J., 1984, ApJ 287, 341
Ferch *R.*L., Salpeter E.E., 1975, ApJ 202, 195
Gathier *R.*, 1987, A&AS 71, 245
Hartigan P., Raymond J., Hartmann L., 1987, ApJ 316, 323
Juguet J.L., Louise *R.*, Macron A., Pascoli G., 1988, A&A 205, 267
Kaler J.B., Lutz J.H., 1985, PASP 97, 700
Kaler J.B., Shaw *R.*S., Browning L.B., 1997, PASP 109, 289
Keenan F.P., Aller L.H., Bell K.L., Hyung F.C., MnKenna F.C., Ramsbottom C.A., 1996, MNRAS 281, 1073
Khromov G.S., 1976, Sov. Astron. 20, 543
Kingsburgh *R.*L., Barlow M.J., 1992, MNRAS 257, 317
Kingsburgh *R.*L., English J., 1992, MNRAS 259, 635
Kohoutek L., Bull. Ast. Anst. Czech. 18, 203
Mallik D.C.V., Peimbert M., 1988. Rev. Mex. Astron. Astrofis. 16, 111
Marten H., Schönberner D., 1991, A&A 248, 590
Mathews W.G., 1966, ApJ 143, 173
Mellema G., 1994, A&A 290, 915
Mendez *R.*H., Kudritzki *R.*I., Herrero A., Husfield D., Groth H.G., 1988, A&A 190, 113
Mendez *R.*H., Herrero A., Manchado A., 1990, A&A 229, 152
Mendoza C., 1983, In Planetary Nebulae, IAU Symp.*n*. 103, Flower D. (ed.), p. 245
Mendoza C., Zeippen C.J., 1982, MNRAS 198, 127
Milne D.K., 1979, A&AS 36, 227
Milne D.K., Aller L.H., 1975, A&A 38, 183
Moran A., Luise *R.*, 1990, ASS 168, 255
Pedreros M., 1989, AJ 98, 2146
Peimbert M., 1990, Rev. Mex. Astron. Astrofis. 20, 119
Phillips J.P., Cuesta L., 1996, AJ 111, 1227
Phillips J.P., Cuesta L., 1998, A&A (submitted)
Phillips J.P., Guzman V., 1998, A&AS (in press)
Pottasch S.*R.*, 1996, A&A 307, 561
Pottasch S.*R.*, Zijlstra A.A., 1994, A&A 289, 261
Schmidt-Voigt M., Köppen J., 1987a, A&A 174, 211
Schmidt-Voigt M., Köppen J., 1987b, A&A 174, 223
Stanghellini L., Kaler J.B., 1989, ApJ 343, 811
Stasinska G., 1989, A&A 213, 274
Stasinska G., Gorny S.K., Tylenda *R.*, 1997, A&A 327, 736
Tylenda *R.*, Acker A., Stenholm B., Köppen J., 1992, A&AS 95, 337
Van de Steene G.C., Zijlstra A.A., 1994, A&AS 108, 485
Weinberger *R.*, 1989, A&AS 78, 301
Zhang C.Y., 1995, ApJS 98, 659
Zijlstra A.A., Pottasch S.*R.*, Bignell C., 1989, A&AS 79, 329